Acta Chemica Scandinavica A 37 (1983) 367–381

# X-Ray Diffraction Studies of the Structures of Melts within the System (Ag,K,Na)–($I,NO_3$)

BERTIL HOLMBERG [a] and GEORG JOHANSSON [b]

[a] Physical Chemistry 1, Chemical Center, P.O. Box 740, S-220 07 Lund 7, Sweden and [b] Department of Inorganic Chemistry, Royal Institute of Technology, S-100 44 Stockholm 70, Sweden

The structures of 11 melts of different compositions in the system (Ag,K,Na)–($I,NO_3$) have been studied by X-ray diffraction methods at 280 °C. For pure $AgNO_3$ and $AgNO_3$–$(K,Na)NO_3$ mixtures the scattering data indicate a preferred orientation of the nitrate groups around the silver ions with one O closely bonded (2.45 Å) and another O more distant (3.0 Å). For the binary mixed anion system AgI–$AgNO_3$ a model based on a close-packed arrangement of the $I^-$ and $NO_3^-$ ions, with $Ag^+$ occupying tetrahedral holes can explain the scattering data over the whole range of compositions investigated. This is similar to the anion arrangement in the solids $Ag_2INO_3$ and $Ag_3I(NO_3)_2$ in which, however, the $Ag^+$ ions occupy octahedral holes.

For systems AgI–$AgNO_3$–$(K,Na)NO_3$ the short-range cationic arrangement around each $I^-$ is characterized by about four distinct Ag–I distances of 2.8 Å irrespective of the overall $Ag^+$ fraction (0.38 and 0.75). The non-random cation distribution is consistent with previous thermodynamic data. No specific Ag–Ag correlations in the coordination sphere of $I^-$ can be observed, however.

The formation of cationic complexes $Ag_2I^+$, $Ag_3I^{2+}$, and $Ag_4I^{3+}$ has been proposed by different authors to account quantitatively for the increase in solubility of AgI with increasing concentration of $Ag^+$ in aqueous $AgClO_4$ and $AgNO_3$ solutions.[1,2] The existence of complex cations $Ag_mX^{(m-1)+}$ in binary melts AgX–$AgNO_3$ was suggested by Schwartz already in 1941,[3] and dinuclear silver halide species $Ag_2X^+$ have often been considered in tests of the quasi-lattice models for ternary melts, dilute in $Ag^+$ and $X^-$. This field of chemistry has been briefly reviewed by Holmberg.[4]

From a recent study [5] of the solubility of AgI at 280 °C in molten equimolar mixtures of $KNO_3$ and $NaNO_3$, containing various amounts of $AgNO_3$, it was concluded that silver and iodide form a series of complex ions $Ag_mI^{(m-1)+}$, with formal charges of +1, +2 and +3. This conclusion was supported by emf measurements of the Ag(I) activity as a function of $I^-$ added to $(K,Na)NO_3$ melts with a high concentration of $AgNO_3$. The average number $\overline{m}$ of Ag(I) in the cationic complexes was estimated to be 3.5–4.0 [5] and the thermodynamic stability of cationic silver iodide complexes in molten $(K,Na)NO_3$ would thus be of the same order of magnitude as that of anionic species, $AgI_n^{(n-1)-}$.

The structure of complex cations of this kind is not known and the present study was made in an attempt to clarify the arrangement of $Ag^+$ ions around the iodide ions in melts of various compositions in the quasi-ternary system Ag,(K,Na)–$I,NO_3$ and in the binary subsystems AgI–$AgNO_3$. The temperature chosen for the investigation was the same as that used for the equilibrium measurements, *i.e.* 280 °C. In a parallel research project the crystal structures of a number of compounds $Ag_mX_nA_y$ (X=halide, A=other anion, $m>n$) have been determined,[6] including $Ag_2ClNO_3$,[7] $Ag_2BrNO_3$,[8] $Ag_2INO_3$,[9] $Ag_3I(NO_3)_2$,[10] $Ag_2IF \cdot H_2O$,[11] $Ag_7I_2F_5 \cdot 2.5H_2O$[12] and $Ag_3I(ClO_4)_2$.[13] The structure of the analogous compound $Ag_{13}I_9(WO_4)_2$ is also known.[14] No uniform geometrical arrangement of $Ag^+$ around the halide atoms is found,

0302-4377/83 $02.50

however, in these structures. In $Ag_2ClNO_3$ and $Ag_2BrNO_3$ each $Cl^-$ and $Br^-$ is surrounded by five Ag forming a trigonal bipyramid. In $Ag_2INO_3$ and $Ag_3I(NO_3)_2$ six $Ag^+$ form distorted trigonal prisms around $I^-$. In the fluoride and the perchlorate compounds no well-defined $Ag^+$ coordination geometry around $I^-$ seems to occur, and $Ag_{13}I_9(WO_4)_2$ is an ionic conductor with $Ag^+$ freely moving within a network of iodide tetrahedra. Structural relations between the compounds can, however, be found by considering the packing of the anions, which, for example, in $Ag_2INO_3$, $Ag_3I(NO_3)_2$ and $\beta$-$AgNO_3$ (the high-temperature modification of silver nitrate [15]) can be described as close-packed arrangements with $Ag^+$ ions occupying available holes.

X-Ray diffraction data for 11 different compositions of melts in the Ag,(K,Na)–I,$NO_3$ system will be presented and discussed in the present paper. It follows from the 553 K isotherm for this system [16] that at this temperature binary melts $AgI-AgNO_3$ can be studied over the composition range $0 \leqq X_I \leqq 0.74$, $X_I$ being the anion fraction of iodide. The general structural change caused by a gradual replacement of $NO_3^-$ with $I^-$ has been followed from pure liquid $AgNO_3$ to a melt of composition $AgI_{2/3}(NO)_{1/3}$. Two of the compositions investigated were chosen to correspond to those of the crystalline compounds $Ag_2INO_3$ and $Ag_3I(NO_3)_2$ (melting points: 109 and 119 °C, respectively [17]) to allow a direct comparison with the structure of the solids. Previous diffraction studies of multicomponent ionic melts are limited to binary systems with a common anion and the present study seems to be the first report on X-ray diffraction in mixed anion melts. Ternary melts $(K,Na)NO_3-AgI-AgNO_3$ have also been included in the investigation. In order to obtain sufficiently high iodide concentrations in these melts, we have worked with systems having contents of $AgNO_3$ considerably higher than those used in the thermodynamic study.[5] A straightforward extrapolation of the thermodynamic data into this range gives a ligand ($Ag^+$) number $\bar{m} \approx 4$, *i.e.* each $I^-$ should on an average have four $Ag^+$ as nearest neighbours irrespective of the overall cationic $Ag^+$ fraction in the melts.

An analysis of the radial distribution functions (RDF) for the ternary melts requires information on the RDFs for simpler subsystems of similar compositions. Accordingly, binary melts $(K,Na)NO_3-AgNO_3$ and $(K,Na)NO_3-(K,Na)I$ as well as pure equimolar $(K,Na)NO_3$ have also been investigated. Previous structure information on such nitrate melts has emerged essentially from spectral studies and diffraction measurements on single component molten salts.

Although numerous studies of vibrational spectra have presented evidence for strong interactions between silver and nitrate ions in pure liquid $AgNO_3$ and mixtures with alkali metal nitrates,[18–33] no precise information on the nature of the silver-nitrate interaction is available. The spectral characteristics have been considered as due to collective vibrational motions of a quasi-lattice-like structure. The lowering of the nitrate ion symmetry to $C_{2v}$ or $C_s$, which is generally observed, has also been attributed to the existence of specific contact ion pairs in the melt.[22] Brooker [32] recently considered non-equivalent sets of nitrate ions in molten $AgNO_3$– one associated with a particular cation and one in a non-specific cation environment. Clarke [29] attributed the $AgNO_3$ Raman band at 107 $cm^{-1}$ to a librational oscillation of the nitrate ion around the $C_2$ axis due to restricted out-of-plane rotation and concluded that $Ag^+$ is capable of simultaneous association with more than one nitrate ion in mixtures with alkali metal nitrate.

Suzuki and Fukushima [34] investigated the structure of the nitrate ion in pure molten $AgNO_3$ from pulsed neutron diffraction data and found slightly different O–O distances in $NO_3^-$ giving a $C_{2v}$ symmetry. Previous X-ray diffraction studies of related molten salt systems include single component $AgNO_3$ and alkali metal nitrates only.[35–38] Ohno and Furukawa [37] studied molten $AgNO_3$ at 260 °C and proposed a simple cubic (NaCl-like) packing arrangement of ions, but no specific conclusion about any preferential $Ag^+-NO_3^-$ interaction geometry could be drawn from their data.

## EXPERIMENTAL

All melts were prepared from *p.a.* grade chemicals, predried, fused under vacuum, purged with dry $N_2$ and filtered as described previously.[39] The mass density was determined volumetrically in a Pyrex glass vessel, calibrated with $AgNO_3$ by use of the data of Boardman *et al.*[40]

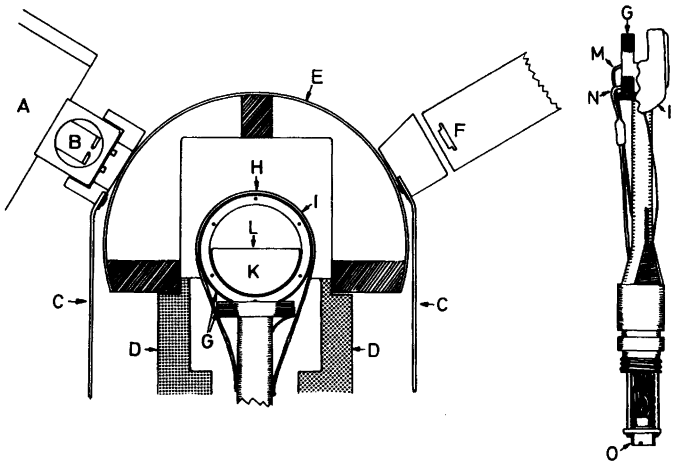


*Fig. 1.* The experimental arrangement used for the molten salt diffraction measurements. A, X-ray tube; B, Zoller slit; C, lead rubber protection; D, water-cooled metal cylinder; E, beryllium window; F, scatter slit; G, thermocoax heating coil; H, aluminum framed Al window; I, aluminum covered glass fiber; K, glass fiber reinforced teflon container; L, melt; M, Fe-const. thermocouple; N, Pt-100 element; O, connector.

The arrangement used to keep the melt at a constant temperature, usually 280 °C, during the scattering measurements is illustrated in Fig. 1. The sample was kept in a glass-fiber reinforced teflon container shaped as a half cylinder with the open surface 25×30 mm and a depth of 20 mm. It was placed inside a cylinder of aluminum provided with a thermocoax heating element (~25 Ω) and isolated from the surroundings by a layer of glass fiber covered by aluminum foil. An opening for the X-rays about 15 mm wide was covered by 0.01 mm thick aluminum foil. This isolated chamber was positioned inside a cylindrical radiation shield having a 15 mm wide opening for the X-rays covered with a 0.5 mm thick beryllium window. A copper-constantan thermocouple and a Pt-100 resistance thermometer, placed close to the teflon container, were used to measure the temperature. The resistance thermometer also served as a sensor to regulate the temperature which could be kept constant within ±0.1 °C from a preselected value.

The diffractometer has been described in previous papers.[41] Mo$K\alpha$ radiation ($\lambda$=0.7107 Å) was used for the diffraction measurements. The radiation scattered from the free surface of the melt was reflected in a curved single crystal monochromator of lithium fluoride before being measured in a scintillation counter provided with a pulse height discriminator. The scattered radiation was measured at discrete intervals of 0.1° for $1°<\theta<20°$ and 0.25° for $20°<\theta<70°$. Three different slit combinations were used to cover the entire $\theta$ region. For each point 100 000 counts were collected and each melt was scanned twice, which corresponds to a statistical error of 0.22 % in observed intensity values. Corrections were made for absorption when necessary, for polarization in the sample and in the monochromator, for contributions from incoherent scattering slipping through the monochromator and for multiple scattering. Normalization to a stoichiometric unit of volume containing one formula weight of MX (M=Ag, Na, K and X=$NO_3$, I) was done by comparing measured intensities in the high-angle region with calculated values for the sum of independent coherent and incoherent scattering. Reduced intensities $i(s)$, where $s=4\pi\lambda^{-1}\sin\theta$, were obtained as

$$i(s) = KI(s) - \sum_{i=1}^{N} n_i \{(f_i(s)+\Delta f_i')^2+(\Delta f_i'')^2+\mathrm{del}(s)I_i^{\mathrm{incoh}}(s)\}$$

Here $K$ is the normalization factor, $I(s)$ the observed intensities corrected for absorption, polarization, and multiple scattering, $N$ is the number of different atomic species in the melt, $n_i$ the number of atoms "$i$" in the stoichiometric unit of volume, $f_i(s)$ the scattering factors for atom "$i$", $\Delta f_i'$ and $\Delta f_i''$ the real and the imaginary parts of the anomalous dispersion corrections, $I_i^{\mathrm{incoh}}(s)$ the incoherent scattering and del($s$) the

estimated fraction of incoherent scattering passing through the monochromator. The del($s$) function was estimated from the spectrum of the X-ray tube and was checked in the high-angle region by comparing measurements done with a Zr filter placed before and after the sample, respectively.

Scattering factors, $f_i(s)$, for the neutral atoms were used.[42,43] Anomalous dispersion corrections, $\Delta f_i'$ and $\Delta f_i''$, were taken from Cromer.[44] Values for incoherent scattering were those given by Cromer.[45] Corrections for the Breit-Dirac factors were applied. All calculations were done with the use of programs described previously.[46]

The reduced intensities were corrected for low-frequency contributions leading to spurious peaks in the D(r) functions below about 1 Å and not ascribable to interatomic distances.[46] The electronic radial distribution functions were calculated from the expression:

$$D(r) = 4\pi r^2\rho_o + \frac{2r}{\pi}\int_0^{s_{max}} si(s)\,(\sin rs)M(s)\mathrm{d}s$$

with the modification function

$$M(s) = [f_I^2(0)/f_I^2(s)]\,\exp(-0.01\,s^2).$$

For an assumed structural model, theoretical intensities were calculated from the Debye expression for discrete intramolecular interactions:

$$i(s)_{calc} = \sum_p \sum_q f_p(s)f_q(s)\frac{\sin(s\,r_{pq})}{sr_{pq}}\exp(-b_{pq}s^2).$$

$r_{pq}$ is the distance between the atoms $p$ and $q$, and $b_{pq}$ is related to the rms variations $l_{pq}$ of the distance: $b_{pq}=1/2\cdot l_{pq}^2$. Intermolecular interactions were approximated by assuming an evenly distributed electron density outside a sphere of radius $R$.[46] Corresponding shape functions were calculated by a Fourier inversion analogous to the one used for the experimental intensity data.

Compositions of the melts investigated are given in Table 1 and are indicated in the phase diagrams in Fig. 2.

## RESULTS AND DISCUSSION

*Systems $AgNO_3$–(K,Na)$NO_3$.* Changes in the radial distribution curves caused by a gradual replacement of the cations in equimolar (K,Na)$NO_3$ by $Ag^+$ from (K,Na)$NO_3$(l) to $AgNO_3$(l) are illustrated in Fig. 3 for the melts A to D.

*Table 1.* Compositions of the melts investigated.

| | Melt | Density/(g cm$^{-3}$) | Stoichiom. vol., $V$/Å$^3$ | Ag mol l$^{-1}$ | Atoms in V | (K,Na) mol l$^{-1}$ | Atoms in V | $NO_3$ mol l$^{-1}$ | Atoms in V | I mol l$^{-1}$ | Atoms in V |
|---|---|---|---|---|---|---|---|---|---|---|---|
| A | (K,Na)$NO_3$ | 1.918±0.004 | 80.5 | | | 20.62 | 1 | 20.61 | 1 | | |
| B | $Ag_{0.38}(K,Na)_{0.62}NO_3$ | 2.663±0.006 | 76.1 | 8.24 | 0.378 | 13.56 | 0.622 | 21.81 | 1 | | |
| C | $Ag_{0.75}(K,Na)_{0.25}NO_3$ | 3.390±0.007 | 74.0 | 16.92 | 0.754 | 5.53 | 0.246 | 22.45 | 1 | | |
| D | $AgNO_3$ | 3.890 | 72.5 | 22.90 | 1 | | | 22.90 | 1 | | |
| E | $Ag_6I(NO_3)_5$ | 4.202±0.008 | 71.4 | 23.26 | 1 | | | 19.38 | 0.833 | 3.88 | 0.167 |
| F1 | $Ag_3I(NO_3)_2$ 280 ° | 4.536±0.008 | 70.1 | 23.68 | 1 | | | 15.79 | 0.667 | 7.89 | 0.333 |
| F2 | $Ag_3I(NO_3)_2$ 140° | 4.861±0.008 | 65.4 | 25.38 | 1 | | | 16.92 | 0.667 | 8.45 | 0.333 |
| G | $Ag_2INO_3$ | 4.869±0.010 | 69.0 | 24.06 | 1 | | | 12.03 | 0.500 | 12.03 | 0.500 |
| H | $Ag_3I_2NO_3$ | 5.203±0.010 | 68.0 | 24.41 | 1 | | | 8.14 | 0.333 | 16.27 | 0.667 |
| I | $(K,Na)I_{0.05}(NO_3)_{0.95}$ | 1.974±0.005 | 81.2 | | | 20.44 | 1 | 19.35 | 0.946 | 1.097 | 0.054 |
| J | $Ag_{0.38}(K,Na)_{0.62}I_{0.05}(NO_3)_{0.95}$ | 2.628–0.006 | 79.4 | 7.91 | 0.378 | 13.02 | 0.622 | 19.80 | 0.946 | 1.123 | 0.054 |
| K | $Ag_{0.75}(K,Na)_{0.25}I_{0.05}(NO_3)_{0.95}$ | 3.495±0.008 | 73.4 | 17.05 | 0.754 | 5.57 | 0.246 | 21.41 | 0.946 | 1.214 | 0.054 |

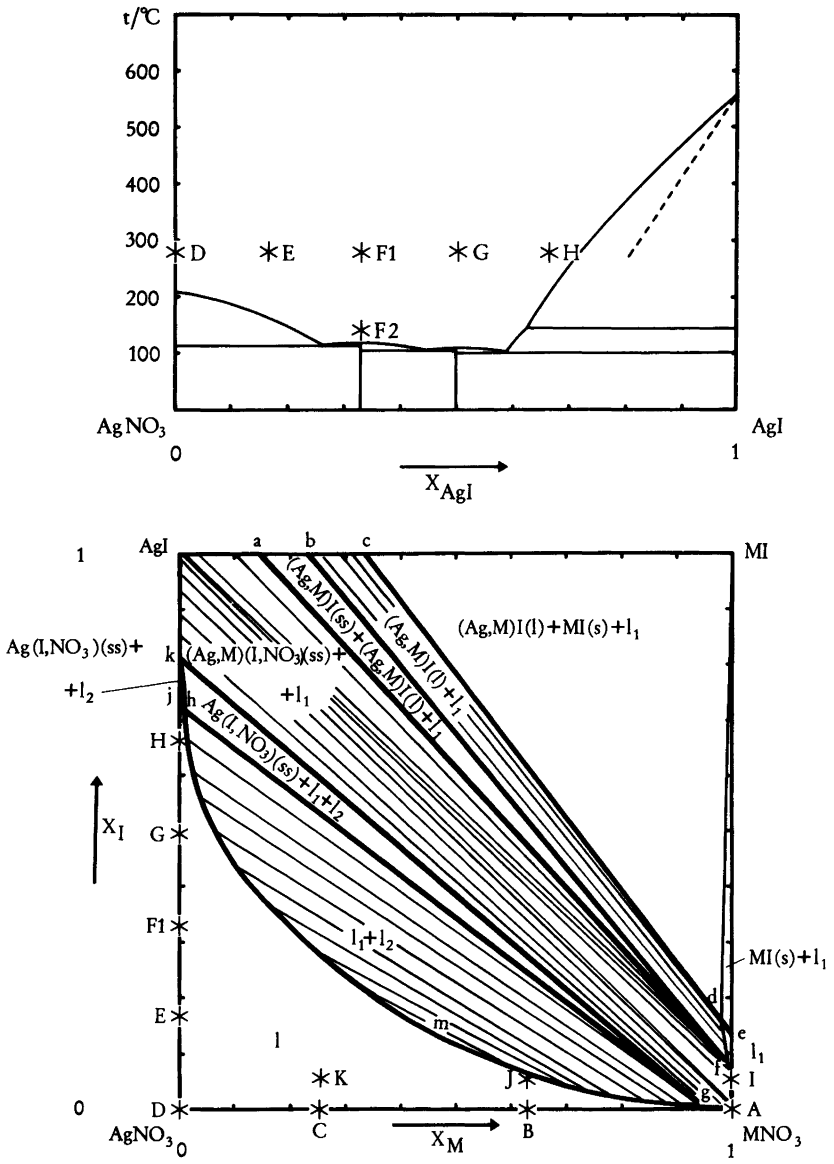


*Fig. 2.* (a) Phase diagram for the $AgNO_3$–AgI system constructed from data of Refs. 5 and 17. (b) The M,Ag–I,$NO_3$ isotherm at 280 °C (M=(K,Na)) from Ref. 16. The compositions of all investigated melts are indicated.

The first two peaks in the RDF for pure (K,Na)$NO_3$ (=A) are observed at 1.2 and 2.1 Å, corresponding to the expected N–O and O–O distances within the nitrate ion. The corresponding peaks for the melts B to D are much less pronounced because of the large concentration of $Ag^+$ in these systems. The interatomic distances within the planar nitrate ion, which have been used in the model calculations, were set to N–O=1.24 Å and O–O=2.14 Å in accordance with these and previous findings.

For (K,Na)$NO_3$ the next two peaks occur at about 2.9 Å and 4.3 Å. The first of these most probably corresponds to cation–$NO_3^-$ interac-

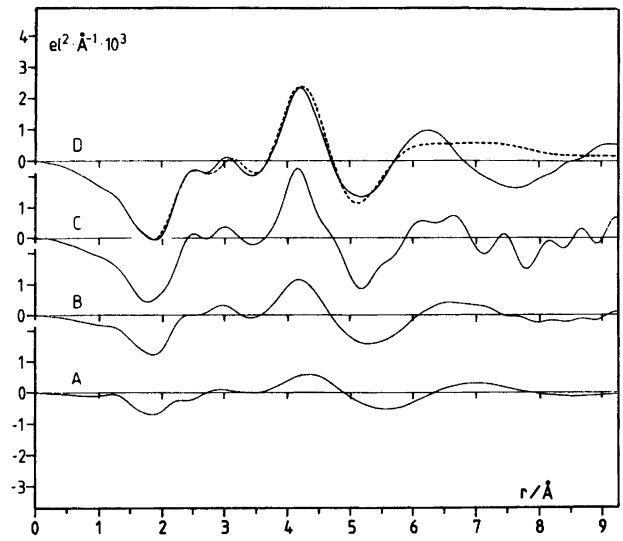


*Fig. 3.* $D(r)-4\pi r^2\rho_0$ functions for the melts A to D (see Table 1 and Fig. 2). The dashed line for "D" is a theoretical curve calculated with parameter values given in Table 2.

tions. For pure $NaNO_3$(l) (340 °C) and $KNO_3$(l) (360 °C) the corresponding distance has been reported to be 2.65 and 3.00 Å, respectively.[37] In the mixed cation system (K,Na)$NO_3$ these two peaks are not resolved and only one broad peak with a maximum at the intermediate value of 2.9 Å appears. The maximum at 4.3 Å also falls between the values 4.00 and 4.35 Å, previously reported for $NaNO_3$(l) and $KNO_3$(l). These features indicate that the modified close-packed type of ionic arrangement suggested by Ohno and Furukawa [37] for the single component melts might also be a good model description of the mixed alkali metal nitrate melt.

The changes in the radial distribution function caused by replacing alkali metal ions in (K,Na)$NO_3$ with $Ag^+$ are illustrated in Fig. 3. An increasing fraction of $Ag^+$ from 0.38 in "B" to 1.0 in "D" results in increasing peaks at about 2.5 Å, 3.0 Å and 4.2 Å. In crystals, such as $Ag_2INO_3$,[4] $Ag_3I(NO_3)_2$,[10] $\beta$-$AgNO_3$ [15] and $KAg(NO_3)_2$,[47] nitrate groups are often found to be coordinated to $Ag^+$ in the way illustrated in Fig. 4. One oxygen is closely bonded with an Ag–O distance of about 2.5 Å. Another oxygen occurs at a distance of about 3.0 Å, approximately the same as the Ag–N distance, and the third Ag–O distance is about 4.2 Å. The radial distribution curves in Fig. 3 seem to indicate a similar coordination in molten $AgNO_3$ and $AgNO_3$–(K,Na)$NO_3$ mixtures.

Two crystalline modifications of $AgNO_3$ have been described and their crystal structures have been determined. In the modification stable at room temperature,[48] $Ag^+$ ions are joined by shared nitrate groups into pairs with an Ag–Ag distance of 3.22 Å, not much longer than the distance of 2.89 Å found in silver metal. Similar short Ag–Ag distances occur in several other silver compounds.[11] The other modification, $\beta$-$AgNO_3$, is unstable at room temperature but can be obtained by rapid supercooling of molten $AgNO_3$. Here the shortest Ag–Ag distances are 4.06 Å and each Ag atom is in close contact (2.45–2.58 Å) with six nitrate oxygens.[15]

The scattering data from the $AgNO_3$ melt can be closely reproduced by a model in which an $Ag^+$ ion is assumed to coordinate about four

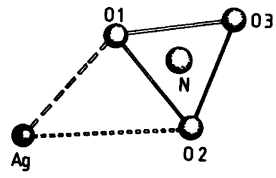


*Fig. 4.* Suggested model for the coordination of a nitrate group to $Ag^+$.

nitrate groups in the way shown in Fig. 4. This is sufficient to explain the peaks at 2.5 Å and 3.1 Å in the distribution curves for $AgNO_3$(l) and the presence of short Ag–Ag distances of the type found in many crystals does not have to be assumed. This is shown by the comparison in Fig. 3 of calculated and experimental $D(r)-4\pi r^2\rho_o$ functions for $AgNO_3$(l) (="D"). The parameters used for the theoretical model are given in Table 2 and assume all nitrate groups to be coordinated in the same way with $Ag^+$ in the plane of the group. The rather limited information contained in the scattering data does not justify a more detailed model in particular, since the light atom interactions cannot be distinguished as separate peaks. Also the calculations are not sensitive towards limited movements of the $Ag^+$ ion out of the plane of the nitrate group. Thus, the scattering data for $AgNO_3$(l) are consistent with a model with a preferred orientation of the nitrate groups around $Ag^+$ with frequent Ag–O interactions occurring at about 2.45 Å and 3.0 Å. Significant deviations from this geometry for a large number of nitrate groups are unlikely as

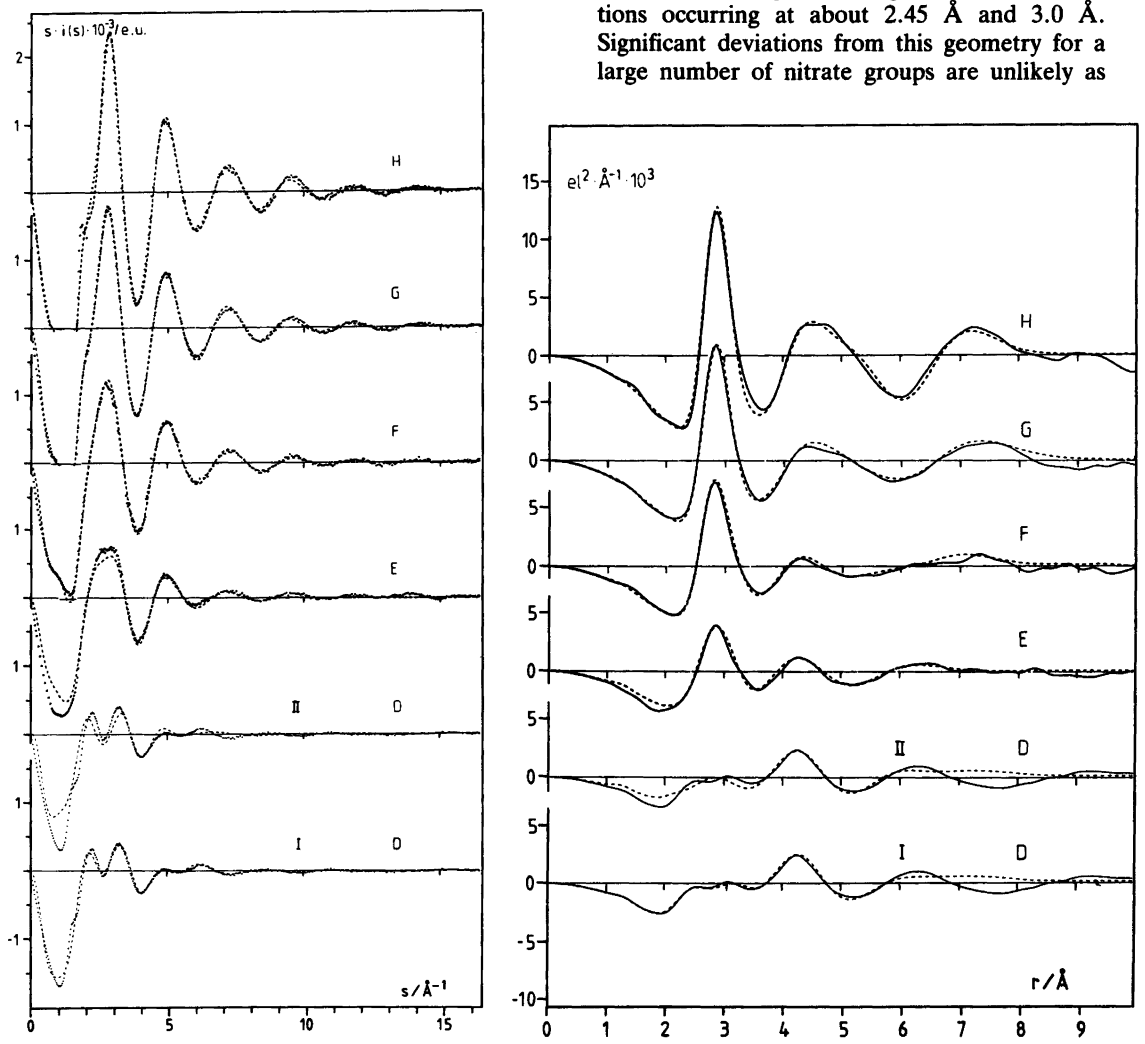


*Fig. 5.* (a) Comparison between observed (dots) and calculated (dashes) $s\cdot i(s)$ functions for the melts D to H (see Table 1 and Fig. 2). Parameters used for the theoretical curves are given in Table 4 for DII, E, F, G and H and in Table 2 for DI. (b) Corresponding observed (solid lines) and calculated (dashed lines) $D(r)-4\pi r^2\rho_o$ functions.

*Table 2.* Parameters used for the model calculations for $AgNO_3$(l) in Fig. 3 (D) and Fig. 5 (D:I). The assumed Ag–$NO_3$ coordination is illustrated in Fig. 4. $d$=interatomic distance in Å, $b$=temp. coeff. in Å$^2$, and $n$=number of interactions referred to one Ag atom. $R$=the radius in Å for the emergence of the continuum and B=the corresponding temp. coefficient.

| | $d$ | $b$ | $n$ | $R$ | $B$ |
|---|---|---|---|---|---|
| Ag–N | 3.13 | 0.04 | 3.8 | | |
| Ag–O1 | 2.45 | 0.022 | 3.8 | | |
| Ag–O2 | 3.05 | 0.022 | 3.8 | | |
| Ag–O3 | 4.32 | 0.06 | 3.8 | | |
| Ag–Ag $NO_3$–$NO_3$ | 4.07 | 0.17 | 3.5 | | |
| Ag–$NO_3$ | 5.4 | 0.2 | 8.3 | | |
| $Ag^+$ | | | | 5.5 | 0.4 |
| $NO_3^-$ | | | | 5.5 | 0.4 |

they should result in other peaks than those now observed in the region between 2.5 and 4 Å in the RDF. Freely rotating or randomly oriented nitrate groups cannot explain the two peaks at 2.5 and 3.2 Å, as shown by the comparison in Fig. 5 (DII), which will be discussed later. In the crystal structure of $MAg(NO_3)_2$ (M=K,$NH_4$ or Rb) [47] and in the high temperature form $\beta$-$AgNO_3$, nitrate groups are coordinated approximately as shown in Fig. 4 and for Ag atoms sharing nitrate oxygens the shortest Ag–Ag distances are ~4.1 Å. This distance corresponds to the position of the dominant peak at 4.1 Å in the RDFs for the Ag containing melts (Fig. 3), which has, therefore, been identified with Ag–Ag interactions in the model used (Table 2).

The $D(r)-4\pi r^2\rho_0$ functions for the melts "B" and "C" in Fig. 3 show that the same type of $Ag^+$–$NO_3^-$ interaction occurs in the mixed $AgNO_3$–(K,Na)$NO_3$ melts.

*Systems AgI–AgNO$_3$.* Addition of AgI to $AgNO_3$(l) results in a marked peak at about 2.8 Å in the distribution curves which can be related to Ag–I contact distances in the melts. Other changes are less pronounced as seen by a comparison between the distribution curves given

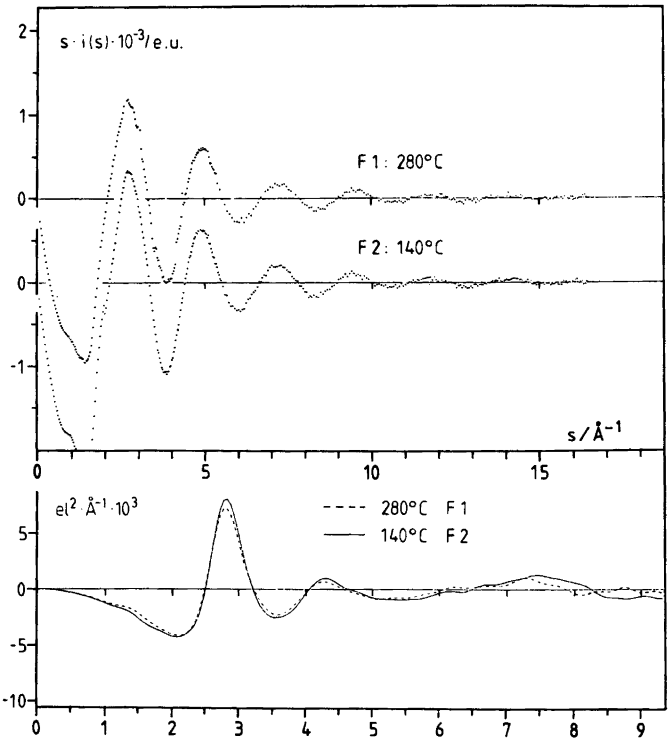


*Fig. 6.* Comparison between observed $si(s)$ values and $D(r)-4\pi r^2\rho_0$ functions for the melt F at two different temperatures.

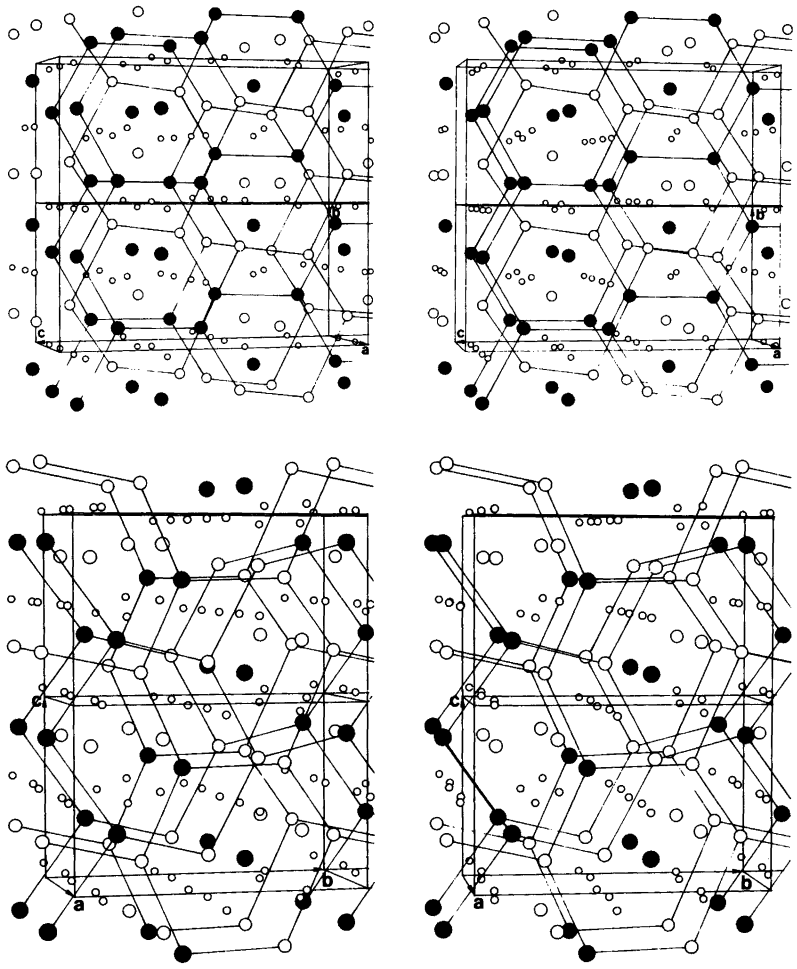

*Fig. 7.* Stereoscopic views of the ion packings in $Ag_2INO_3$ (a) and $Ag_3I(NO_3)_2$, (b). Large circles are $I^-$ (filled) and N (open), and small circles represent the $Ag^+$ positions. The oxygens of the $NO_3^-$ groups are omitted.

in Fig. 5b.

For two of the melts investigated, "F" and "G" in Fig. 5, the compositions correspond to the two solid compounds $Ag_3I(NO_3)_2$ and $Ag_2INO_3$ (Fig. 2), the crystal structures of which have been determined.[9,10] For the melt "F" with the composition $Ag_3I(NO_3)_2$ diffraction measurements were also made at 140 °C, which is only about 20 K above the melting point of the solid. A comparison between the results obtained for "F" at the two different temperatures is given in Fig. 6. The peaks in the $si(s)$ and the $D(r)-4\pi r^2\rho_o$ functions are slightly less distinct at the higher temperature, but the differences are minor and seem to be limited primarily to a slight broadening of the Ag–I peak at 2.8 Å towards longer distances. The slightly unsymmetrical broadening is probably due to an increased exchange frequency between nearest Ag–I neighbours at the higher temperature, increasing the upper range of distances in the average distribution, whereas the lower range is limited by repulsive forces. Thus no significant structural change takes place in the melt between 280 °C and the melting point.

By assuming the short range order in the crystals to be retained in the melts, distribution

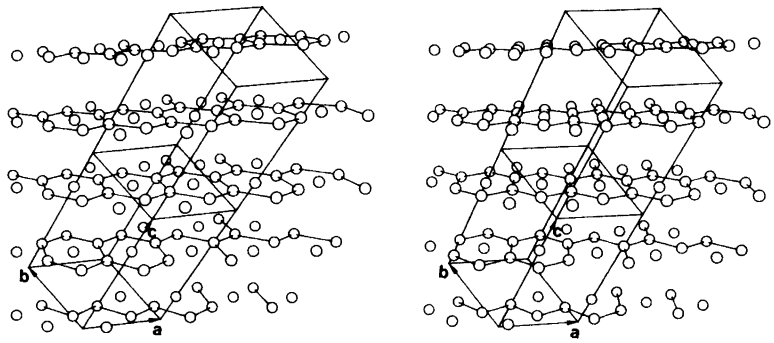


*Fig. 8.* The nitrate ion arrangement in $\beta$-$AgNO_3$, schematically shown by the N positions of the $NO_3^-$ groups.

curves were calculated and were compared with the experimental curves. This comparison showed the degree of order in the melt to be much less than in the crystals. Hence this approach is not very useful for an analysis of the experimental data. It did bring out, however, that the number of Ag–I contacts per I atom is smaller in the melt than in the corresponding crystals and the Ag–I contact distances, which fall in the range 2.865–3.295 Å in the crystals with an average value of 2.99 Å, are shortened to about 2.8 Å in the melts. Also the many Ag–Ag

*Table 3.* Frequency of distances, *d*, in a regular hexagonal close-packing of anions, X, with cations, M, occupying all tetrahedral holes. *R*=radius of the close-packed anion.

| *d*/*R* | M–M | M–X | X–X | *d*/Å values for *R*=2.15 Å | Peaks in D(r) for melts E–H |
|---|---|---|---|---|---|
| 0.816 | 1 | | | 1.75 | |
| 1.225 | | 8 | | 2.63 | 2.8 |
| 1.414 | 3 | | | 3.04 | |
| 2 | 12 | | 12 | 4.30 | 4.2 |
| 2.041 | | 2 | | 4.39 | |
| 2.160 | 6 | | | 4.64 | |
| 2.345 | | 18 | | 5.04 | 5.2 |
| 2.448 | 4 | | | 5.26 | |
| 2.708 | 3 | | | 5.82 | |
| 2.828 | 6 | | 6 | 6.08 | |
| 2.858 | | 12 | | 6.14 | |
| 3.082 | | 18 | | 6.63 | 6.8 |
| 3.162 | 12 | | | 6.80 | |
| 3.266 | 2 | | 2 | 7.02 | |
| 3.367 | 3 | | | 7.24 | |
| 3.464 | 18 | | 18 | 7.45 | |
| 3.559 | 6 | | | 7.65 | |
| 3.674 | | 18 | | 7.90 | |
| 3.830 | 12 | | 12 | 8.23 | |
| 3.851 | | 6 | | 8.28 | |
| 3.916 | 6 | | | 8.42 | |
| 4 | 6 | | 6 | 8.60 | |
| 4.021 | | 12 | | 8.65 | |

distances at around 4 Å in the crystals are much less pronounced in the melts and do not appear as discrete peaks.

For interpreting the distribution curves in terms of a structural model the following approach was found more useful. An analysis of the crystal structures of the two compounds $Ag_2INO_3$ and $Ag_3I(NO_3)_2$ shows that the anions occupy positions corresponding approximately to a hexagonal close-packing with the $NO_3^-$ ions and the $I^-$ ions distributed over the available anion positions. This is demonstrated in Fig. 7, showing stereoscopic views of the structures. The $NO_3^-$ groups are represented by the N positions only, in order to make the overall anion packing more clear. In these close-packed arrangements the $Ag^+$ ions occupy the octahedral holes, which lead to the trigonal prisms of Ag atoms surrounding the anions, which were discussed in the original papers on the crystal structure determinations.[9,10]

In the $\beta$-$AgNO_3$ structure the nitrate ions are arranged in layers of a close-packed type as shown in Fig. 8, but the stacking of the layers differs from that of a close-packed structure.

The peaks in the radial distribution curves for the melts (Fig. 5) occur at distances approximately corresponding to those expected for a close-packed arrangement (Table 3) of the anions. The peak at about 2.8 Å should then correspond to cation–anion distances, the second peak, at 4.2 Å, to anion–anion and cation–cation distances, and the diffuse peak at about 5.2 Å to cation–anion distances. In Table 3 a comparison is made with the expected distribution of distances for a perfect hexagonal close-packing. Very similar values are obtained for a cubic close-packing, since the most prominent differences in packing statistics between hcp and ccp occur for distances larger than $3R$, with $R$ being the radius of the close-packed anion.

For all of the melts, theoretical curves in satisfactory agreement with those observed could be obtained on the basis of this packing model, assuming $I^-$ and $NO_3^-$ ions to be randomly distributed over the anion sites and using spherical symmetric scattering factors for the nitrate ion. An arbitrarily chosen value of $R$=5.5 Å was used

*Table 4.* Parameter values used for the theoretical curves in Fig. 5. X=$I^-$ or $NO_3^-$, assumed to be randomly distributed.

| Type of interaction | Param. | H | G | F1 | E | DII |
|---|---|---|---|---|---|---|
| | *d* | 2.82 | 2.82 | 2.77 | 2.70 | |
| Ag–I | *b* | 0.015 | 0.015 | 0.015 | 0.021 | |
| | *n* | 3.8 | 3.8 | 4.2 | 4.1 | |
| | *d* | 3.10 | 3.10 | 3.10 | 3.00 | 2.9 |
| Ag–$NO_3$ | *b* | 0.015 | 0.015 | 0.015 | 0.021 | 0.08 |
| | *n* | 3.8 | 3.8 | 4.2 | 4.1 | 4.2 |
| | *d* | 3.35 | 3.35 | 3.3 | | |
| Ag–Ag | *b* | 0.03 | 0.03 | 0.03 | | |
| | *n* | 0.9 | 0.3 | 0.2 | | |
| | *d* | 4.23 | 4.19 | 4.19 | 4.12 | 4.07 |
| Ag–Ag<br>X–X | *b* | 0.11 | 0.18 | 0.17 | 0.17 | 0.17 |
| | *n* | 3.5 | 3.8 | 4.0 | 3.6 | 3.5 |
| | *d* | 5.16 | 5.20 | 5.35 | 5.20 | 5.50 |
| Ag–X | *b* | 0.14 | 0.21 | 0.17 | 0.20 | 0.16 |
| | *n* | 6.7 | 6.8 | 6.2 | 5.8 | 7.5 |
| | *d* | 6.8 | 6.9 | 6.5 | 5.9 | |
| Ag–X | *b* | 0.18 | 0.25 | 0.24 | 0.22 | |
| | *n* | 1.5 | 1.5 | 1.2 | 2.0 | |

for the emergence of the continuum around each ion, with a corresponding "temperature coefficient" of $B$=0.4 Å$^2$, also arbitrarily chosen, to account for the diffuseness of the beginning of the continuum. For each melt, the distance, $d$, the temperature coefficient, $b$, and the frequency, $n$, of each interaction, were adjusted until the best fit was obtained. The final parameter values are given in Table 4 and a comparison between observed and calculated curves is given in Fig. 5.

For $AgNO_3$(l) the DII and the DI curves in Fig. 5 demonstrate the differences in the theoretical curves when the coordinated nitrate groups in the model discussed above (Figs. 3 and 4) are replaced by randomly oriented nitrate groups. The poor agreement between calculated and experimental curves, when spherically symmetric nitrate groups are used can be observed also in the high-angle part of the $si(s)$ curves (Fig. 5a) for melt "E", where the $I^-$ concentration is not yet sufficiently large to hide this effect.

Other values for $R$ and $B$ than those used can be chosen, which will affect the parameter values associated with the longer distances but may lead to equally good fits between observed and calculated values. The parameter values obtained for the first coordination sphere will not be affected as long as the limit for the continuum is chosen sufficiently large. The parameter values for the "best fit" (Table 4) are found to be approximately equal for the different melts which means that over the whole range of composition investigated the differences in the $si(s)$ and the $D(r)$ functions (Fig. 5) can be fully accounted for by the changing mol fractions of $I^-$ and $NO_3^-$. The structural change when AgI is introduced into $AgNO_3$(l) thus seems to be limited primarily to a random replacement of $NO_3^-$ ions by $I^-$ on the anion sites.

The analysis shows also (Table 4) that the number of $I^-$ and $NO_3^-$ ions in the first coordination sphere around an $Ag^+$ ion is close to four in all the melts, which indicates that the cations occupy tetrahedral holes in the close-packed arrangement rather than octahedral holes as in the crystal structures. This change in coordination is indicated also by the shortening of the Ag–I bonds to about 2.8 Å in the melts compared to an average value of 2.99 Å in the crystals.

The number of tetrahedral holes in a close-packed arrangement is twice the number of close-packed anions and, therefore, only 50 % of the tetrahedral holes can be occupied by $Ag^+$ ions. For the most iodide rich melts an Ag–Ag interaction at about 3.3 Å, had to be included in the model (Table 4) in order to improve the fit to the experimental data. This may be an indication that in these melts the $Ag^+$ ions tend to occupy two adjacent tetrahedral holes (Table 3) with shared $I^-$, leading to the short Ag–Ag distances found to be present also in many crystal structures.

*Systems $AgI$–$AgNO_3$–$(K,Na)NO_3$.* The coordination around an $I^-$ ion dissolved as (K,Na)I in molten $(K,Na)NO_3$ and $AgNO_3$–$(K,Na)NO_3$ mixtures was studied by comparison of the distribution curves for the melts A, B and C with those for the melts I, J and K (Fig. 2b). This comparison is summarized in Fig. 9.

An introduction of a small amount (~5 mol %) of $I^-$ into the $(K,Na)NO_3$ melt causes only minor changes in the distribution function as seen from the comparison between the melts I and A in Fig. 9. An analogous substitution of $NO_3^-$ by $I^-$ in the $Ag^+$ containing melts B and C leads to significant changes only in the region around 2.8 Å, corresponding to the Ag–I contact distances (Fig. 9). By comparing the size of the 2.8 Å peak as it appears in the difference curves illustrated in Fig. 9, with peaks calculated by assuming each $I^-$ ion to replace an $NO_3^-$ ion in contact with $Ag^+$, it is found to correspond to about four $I^-$–$Ag^+$ contacts per $I^-$ ion. The curves in Fig. 9 show this number to be independent, within the accuracy of the determination, of the total $Ag^+$ cation fraction in the melts. This indicates a non-random distribution of cations over the available cation positions and the $I^-$ ion thus associates preferentially with $Ag^+$. This would seem to be in accordance with the interpretation of thermodynamic data in terms of complex ions $Ag_mI^{(m-1)+}$.[5] An extrapolation of the thermodynamic data into the composition range for the present study gives $Ag_4I^{3+}$ as the dominant species and the interpretation of the thermodynamic and the X-ray diffraction data thus seems to be consistent. However, a remarkable feature in the radial distribution functions for the melts J and K is the virtual absence of significant new contributions from distinct $Ag^+$–$Ag^+$ interactions within the coordination sphere around the $I^-$ ion. Such interactions should be expected in the region around 4.5 Å (4.6 Å for a tetrahedral

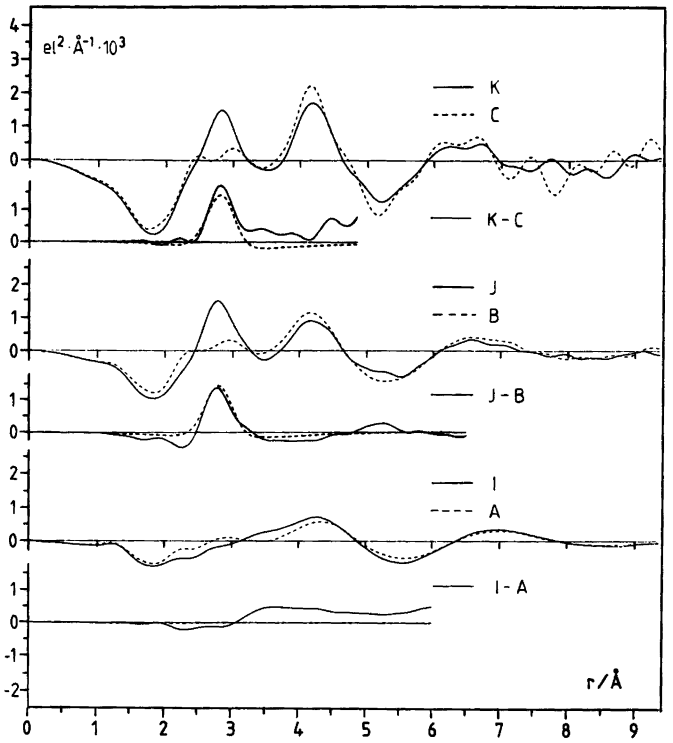


*Fig. 9.* $D(r)-4\pi r^2\rho_o$ function for the melts A, B and C before (dashed lines) and after (solid lines) addition of about 5 mol % $I^-$. Differences between the corresponding $D(r)$ functions are given below (solid lines) and are compared with calculated peak shapes (dashed lines) assuming a nitrate group to be replaced by an $I^-$, bonded to four $Ag^+$.

arrangement, 4.06 Å for a square planar arrangement), where Ag–Ag interactions occur for the iodide-free melts B and C (Table 2 and Fig. 3). Although unlikely, it cannot be excluded that their formation could be balanced by a breaking up of already existing interactions between Ag atoms sharing a nitrate group. The most likely explanation is, however, a considerable tendency to a random spread in Ag–Ag distances among the $Ag^+$ ions in contact with an $I^-$, either becauce of a high mobility or an irregular arrangement of the $Ag^+$ ions within the $I^-$ coordination sphere.

## CONCLUDING REMARKS

It is inherent in the method of liquid X-ray diffraction that it leads to only a one-dimensional representation of the structure, which is not sufficient to resolve the many different types of interactions occurring in a complex system. Even with this limitation, however, valuable structural information can be obtained by following changes in the RDFs with changes in the composition of the system, especially when heavy atoms, which dominate the scattering, are present as the case in the present study.

By comparing the radial distribution functions for various $AgNO_3$–$(K,Na)NO_3$ melts the peaks in the RDFs associated primarily with the $Ag^+$–$NO_3^-$ interactions can be identified, and a model for the interaction geometry can be derived. This is illustrated in Fig. 4 and it is consistent with the arrangement in the solid high-temperature form of $\beta$-$AgNO_3$ as well as in several other crystal structures containing $Ag^+$ and $NO_3^-$ ions. Such a preferential $Ag^+$–$NO_3^-$ arrangement would seem to lower the apparent $NO_3^-$ symmetry in accordance with previous

vibrational spectroscopy findings. A coordination of four $NO_3^-$ to $Ag^+$ in pure molten $AgNO_3$ seems to rule out any description of the melt based on the existence of discrete ion pairs, however, and no distinct nitrate ion symmetry can be deduced from such considerations, since there must be an extensive sharing of $NO_3^-$ ions between $Ag^+$ ions.

The analysis of distribution functions for binary mixed anion melts $AgI-AgNO_3$ has shown that the close-packed arrangement of anions in the solids $Ag_2INO_3$ and $Ag_3I(NO_3)_2$ is retained in the melts, although the order in the melt is effectively averaged out beyond a distance of about $3R$, where $R$ is the radius of the anions. On melting, the $Ag^+$ ions are transferred from the octahedral holes in the solids to a preferential occupation of 50 % of the tetrahedral sites in the corresponding melts.

Changes in the radial distribution functions caused by variations in the $I^-/NO_3^-$ ratio in the $AgI-AgNO_3$ binaries can be satisfactorily accounted for by assuming a random distribution of the two kinds of anions over the sites of a close-packed arrangement. Structural models, based on close-packing geometry, have previously been suggested to account for the structural features of single component molten salts, such as alkali nitrates,[37] sulfates,[49,50] and $ZnCl_2$.[51] The present diffraction study, where mixed anion melts have been investigated for the first time, has thus demonstrated the usefulness of similar approaches to melts with two rather different kinds of close-packed ions.

The results for the quasi-ternary systems $AgI-AgNO_3-(K,Na)NO_3$ indicate a non-random distribution of cations due to a preferential association of $I^-$ with approximately four $Ag^+$ irrespective of the total cation fraction of $Ag^+$ in the melts. This finding is in agreement with a straight-forward extrapolation of thermodynamic data for melts considerably more dilute in $I^-$ and $Ag^+$.[5] On the other hand, no indication of a preferential structural Ag–Ag correlation within a cationic coordination sphere of $I^-$ can be found. Hence, there is no basis for a description of $Ag_mI^{(m-1)+}$ units in these melts by use of classical coordination chemistry concepts. The influence of the structuring properties of the bulk nitrate melt on the total short range order within the closest $I^-$ environment may be of importance. In that perspective, structural studies of analogous systems in other solvents, such as aqueous solutions, should be of value for the clarification of the nature of the proposed $Ag_mI^{(m-1)+}$ species.

*Acknowledgements.* The work has been supported by the Swedish Natural Science Research Council (NFR).

We thank Mr Ernst Hansen for skilful technical assistance.

## REFERENCES

1. Leden, I. and Parck, C. *Acta Chem. Scand. 10* (1956) 535.
2. Lieser, K. H. *Z. Anorg. Allg. Chem. 292* (1957) 114; *Ibid. 304* (1960) 296.
3. Schwartz, K. G. *Z. Electrochem. 47* (1941) 144.
4. Holmberg, B. *Acta Chem. Scand. A 30* (1976) 680.
5. Holmberg, B. *Acta Chem. Scand. A 30* (1976) 797.
6. Persson, K. *Structural Studies on Some Silver(I) and Mercury(II) Halide Compounds in the Solid State,* Thesis, Lund 1981.
7. Persson, K. *Acta Crystallogr. B 35* (1979) 1432.
8. Persson, K. and Holmberg, B. *Acta Crystallogr. B 33* (1977) 3768.
9. Persson, K. *Acta Crystallogr. B 35* (1979) 302.
10. Birnstock, R. and Britton, D. *Z. Kristallogr. 132* (1970) 87.
11. Persson, K. and Holmberg, B. *J. Solid State Chem. 42* (1982) 1.
12. Persson, K. and Holmberg, B. *Acta Crystallogr. B 38* (1982) 1065.
13. Persson, K. and Holmberg, B. *To be published.*
14. Chan, L. Y. Y. and Geller, S. *J. Solid State Chem. 21* (1977) 331.
15. Meyer, P., Rimsky, A. and Chevalier, R. *Acta Crystallogr. B 32* (1976) 1143.
16. Holmberg, B. *Acta Chem. Scand. A 34* (1980) 151.
17. Berg, L. and Lepeshkov, I. N. *Ann. Sect. Anal. Phys. Chim. USSR 15* (1947) 144.
18. Janz, G. J. and James, D. W. *J. Chem. Phys. 35* (1961) 739.
19. Wilmshurst, J. K. and Senderoff, S. *J. Chem. Phys. 35* (1961) 1078.
20. Walrafen, G. E. and Irish, D. E. *J. Chem. Phys. 40* (1964) 911.
21. Janz, G. J. and Kozlowski, T. R. *J. Chem. Phys. 40* (1964) 1699.
22. Wait, S. C., Ward, A. T. and Janz, G. J. *J. Chem. Phys. 45* (1966) 133.

23. Wait, S. C. and Ward, A. T. *J. Chem. Phys. 44* (1966) 448.
24. Devlin, J. P., Williamson, K. and Austin, G. *J. Chem. Phys. 44* (1966) 2203.
25. Li, P. and Devlin, J. P. *J. Chem. Phys. 49* (1968) 1441.
26. Vallier, J. *J. Chim. Phys. Phys.-Chim. Biol. 65* (1968) 1762.
27. James, D. W. and Leong, W. H. *J. Chem. Phys. 51* (1969) 640.
28. Clarke, J. H. R. *Chem. Phys. Lett. 4* (1969) 39.
29. Clarke, J. H. R. and Hartley, P. J. *J. Chem. Soc. Faraday Trans. 2, 68* (1972) 1634.
30. Eluard, A., Balasubrahmanyam, K. and Janz, G. *J. Chem. Phys. 59* (1973) 2756.
31. Kawamura, K. *Trans. Jpn. Inst. Met. 16* (1975) 281.
32. Huang, C.-H. and Brooker, M. *Spectrochim. Acta A 32* (1976) 1715.
33. Prisyazhnyi, V. D., Baranov, S. P. and Kirillov, S. A. *Ukr. Khim. Zh. 45* (1979) 387.
34. Suzuki, K. and Fukushima, Y. *Z. Naturforsch. A 32* (1977) 1438.
35. Danilov, V. I. and Krasnitskii, S. I. *Dokl. Akad. Nauk SSSR 101* (1955) 661.
36. Furukawa, K. *Discuss. Faraday Soc. 32* (1961) 53.
37. Ohno, H. and Furukawa, K. *J. Chem. Soc. Faraday Trans. 1, 74* (1978) 297.
38. Shvets, V. S. and Klintsov, N. Ya. *Ukr. Khim. Zh. 46* (1980) 1152.
39. Hemmingsson, S. and Holmberg, B. *Inorg. Chem. 19* (1980) 2242.
40. Boardman, N. K., Dorman, F. H. and Heyman, E. *J. Phys. Chem. 53* (1949) 375.
41. Johansson, G. *Acta Chem. Scand. 25* (1971) 2787; *20* (1966) 553.
42. Cromer, D. T. and Waber, J. T. *Acta Crystallogr. 18* (1965) 104.
43. *International Tables for X-Ray Crystallography*, Kynoch Press, Birmingham 1968 (Vol. 3) and 1974 (Vol. 4).
44. Cromer, D. T. *Acta Crystallogr. 18* (1965) 17.
45. Cromer, D. T. *J. Chem. Phys. 50* (1969) 4857.
46. Johansson, G. and Sandström, M. *Chem. Scr. 4* (1973) 195.
47. Zobetz, E. *Monatsh. Chem. 111* (1980) 1253.
48. Meyer, P., Rimsky, P. and Chevalier, R. *Acta Crystallogr. B 34* (1978) 1457.
49. Ohno, H. and Furukawa, K. *J. Chem. Soc. Faraday Trans. 1, 74* (1978) 795.
50. Morikawa, H., Miyake, M., Okada, K., Ohno, H. and Furukawa, K. *J. Chem. Soc. Faraday Trans. 1, 76* (1980) 1185.
51. Triolo, R. and Narten, A. H. *J. Chem. Phys. 74* (1981) 703.

Received September 13, 1982.